

PREPARATION AND RECOVERY OF IRON CARBIDE FROM PYRITE CINDER USING CARBURIZATION-MAGNETIC SEPARATION TECHNOLOGY

D. Chen^{a*}, H. Gou^a, Y. Lv^b, P. Li^a, B. Yan^a, J. Xu^a

^a School of Iron and Steel, Soochow University, Jiangsu, China

^b Department of Mechanical and Electrical Engineering, Suzhou Institute of Industrial Technology, Jiangsu, China

(Received 27 April 2018; accepted 04 July 2018)

Abstract

A new technique with carburization followed by magnetic separation is presented for the preparation of high-grade iron carbide from pyrite cinder to promote the high value-added utilization of pyrite cinder. The effects of carburizing temperature, carburizing time and Na_2SO_4 dosage on carburized pellets were investigated, and the effects of Na_2SO_4 dosage and grinding fineness on magnetic concentrate were carried out. The optimized process parameters were proposed as follows: carburizing at 650 °C for 180 minutes in $\text{CO-CO}_2\text{-H}_2$ gas mixtures, Na_2SO_4 dosage of 9%, magnetic field intensity of 130 mT, and grinding fineness of 92.25% powder passing 0.025mm. The iron content, total carbon content, total iron and carbon content of magnetic concentrate were 82.62%, 5.60%, and 88.22%, respectively. The recovery rate of iron reached 88.67%. The behaviors and mechanisms of carburization, separation, and Na_2SO_4 were ascertained with optical microscopy, X-ray powder diffraction (XRD), and scanning electron microscope (SEM).

Keywords: Pyrite cinder; Iron carbide; Carburization; Magnetic separation

1. Introduction

Pyrite cinder produced by roasting pyrite (FeS_2) concentrate is an important secondary iron oxide resource. As a roasted product of pyrite ore, pyrite cinder mainly contains hematite (Fe_2O_3) and magnetite (Fe_3O_4) [1]. However, pyrite ore usually contains a wide range of trace toxic elements, such as Pb, As, and Cd etc. [2, 3], which causes the potential environment problem. Furthermore, the fine size of pyrite cinder often leads to the dust problem in the disposal site. In China, a large amount of pyrite cinder is collected in chemical manufacturing yearly [4], and its stacking has caught acute ecological problems [5-7]. Owing to the low grade of pyrite ore, the iron grade of pyrite cinder is too low to be efficiently utilized. Only a small portion of pyrite cinder has been used in paving, brickmaking, cement, and auxiliary additives [8-12].

Nowadays, most of the pyrite cinder is used to prepare iron ore concentrates, sinter, pellet or sponge iron [1, 13-15] for iron and steel plants. Nevertheless, pyrite cinder is difficult to upgrade and smelt, and the value-added of current utilizing methods of pyrite cinder is low. That is the reason why iron and steel enterprises have no interest in using pyrite cinder, while the iron ore price has decreased in recent years.

Therefore, the utilization of pyrite cinder is still an urgent problem to solve.

Iron carbide is an attractive raw material for steelmaking, and it can also be used for magnetic recording medium, electromagnetic shielding materials, catalyst etc. [16, 17], which possesses higher value-added than iron ore concentrate, sinter, pellet and sponge iron [18]. Several methods for the preparation of iron carbide were reported, such as reaction milling [19], sol-gel [20], laser pyrolysis [21], sonochemistry [22], alkalide reduction [23], chemical vapor condensation [24], and physical vapor deposition [25]. However, the applications of reported methods were restricted by the complex, harsh reaction condition, large energy consumption, low productivity, and high cost corrosive reactants [20, 26]. Compared to the aforementioned approaches, gas phase carburization [27] is the most promising method for the preparation of iron carbide using hematite [28] and magnetite [29] in CO or CH_4 gas, especially for the preparation of steelmaking raw materials.

As an important kind of iron bearing raw material, pyrite cinder also contains hematite and magnetite. Thus, the realization of carburization treatment of pyrite cinder to prepare the iron carbide will greatly promote its utilization. However, due to the low iron

*Corresponding author: chend@suda.edu.cn



grade of pyrite cinder and the absence of separation and refinement techniques, the iron carbide using gas phase carburization prepared from pyrite cinder is difficult to be used as steelmaking raw materials, not to mention the magnetic recording medium, electromagnetic shielding materials or catalyst.

This study focuses on an effective technique to utilize pyrite cinder through the preparation and upgrade of iron carbide. Iron carbide which can be magnetized in magnetic field [17] is similar to the magnetite and iron power. The magnetic separation was demonstrated to be effective for magnetite and iron power recovery from iron ore and solid wastes [30, 31]. For example, magnetite or iron power can be produced from pyrite cinder or low-grade iron ore using magnetizing roasting or direct reduction followed by magnetic separation [1, 32]. Therefore, based on the characteristics of pyrite cinder and iron carbide, in this study a new carburization–magnetic separation treatment is investigated to prepare and upgrade the iron carbide from pyrite cinder. Process parameters were tested and optimized. The new technique was demonstrated to be a feasible way to prepare the high-grade iron carbide from pyrite cinder.

2. Thermodynamic Considerations

The purpose of the carburization is to transform the iron oxides to iron carbide. The carburization mechanism can be expressed by the following reactions [18]:

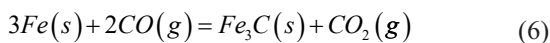
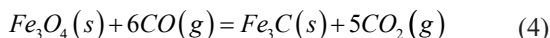
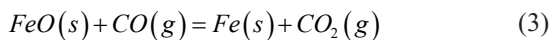
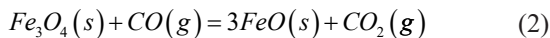
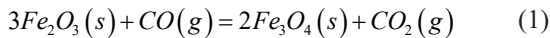


Fig. 1 shows the gas phase equilibrium composition changes of the reduction and carburization reactions. Thermodynamic data was calculated using the thermodynamic software (FactSage 7.0). In Fig. 1, Fe_2O_3 is extremely easy to reduce to Fe_3O_4 . The line of equation (5) is intersected by the lines of equations (4) and (6) at T_1 and T_2 . It can be seen that Fe_3O_4 can be carburized to Fe_3C by CO at the temperature under T_1 , and Fe can be carburized to Fe_3C by CO at the temperature over T_2 . When the temperature is between T_1 and T_2 , Fe_3O_4 is reduced to FeO, and then FeO is carburized to Fe_3C . When the temperature is over T_2 , Fe_3O_4 is reduced to FeO, then FeO is reduced to Fe, and Fe is carburized to Fe_3C finally. In this study, the ratio of $\text{CO}/(\text{CO}+\text{CO}_2)$ is

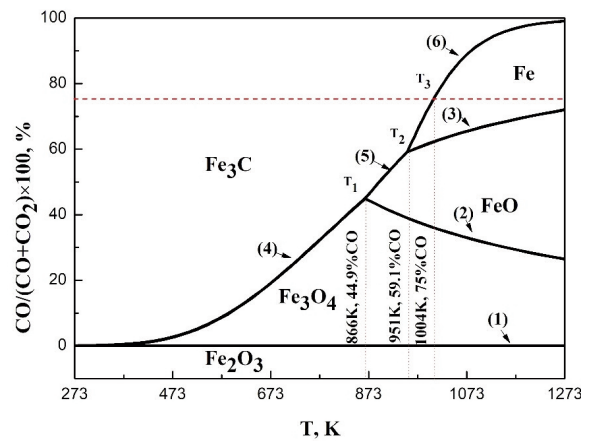
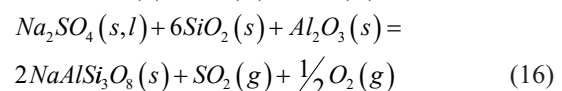
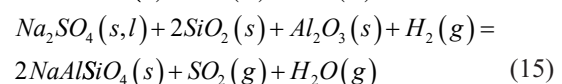
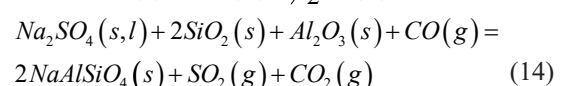
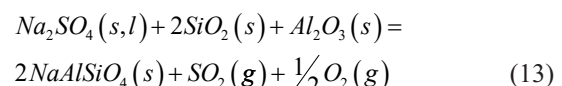
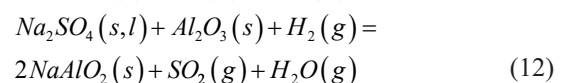
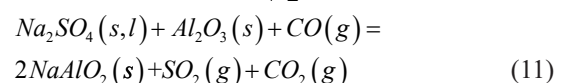
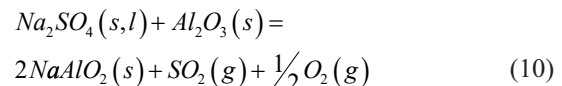
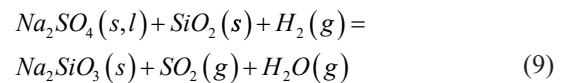
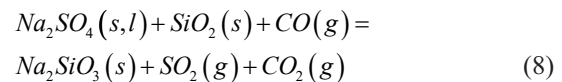
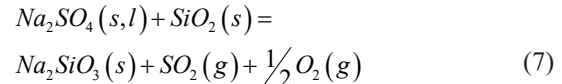
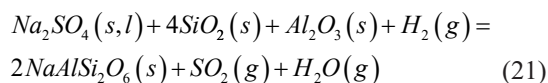
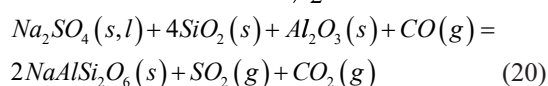
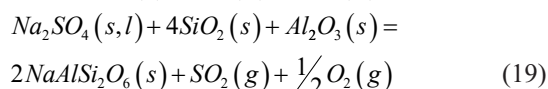
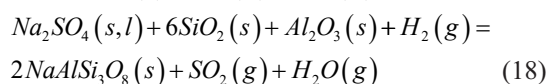
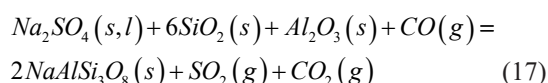


Figure 1. Gas phase equilibrium composition changes of the reduction and carburization reactions

0.75, so the carburizing temperature must be lower than 1004 K. The CO concentrate and reaction temperature of equation (4) is much lower than of equations (5) and (6).

The purpose of the sodium modification is to change the gangue composition of pyrite cinder, which favors separating iron carbon from gangue. The sodium modification mechanisms can be expressed by the following reactions:





comparing these thermodynamic data with Fig. 2, which produces the Na_2SiO_3 , $NaAlSiO_4$, $NaAlSi_3O_8$ and $NaAlSi_2O_6$ more easily except $NaAlO_2$. The standard free energies of reactions (8) and (9) are much lower than that of reactions (11) and (12), and it shows that SiO_2 is easier to modify than Al_2O_3 . When the SiO_2 and Al_2O_3 coexist, the standard free energies of reactions (14), (15), (17), (18), (20) and (21) are lower than that of reactions (8), (9), (11) and (12), and it identifies that coexistence of SiO_2 and Al_2O_3 makes the sodium modify more easily. When the temperature is over 823K, the standard free energies of reactions (17) and (18) are the lowest, the standard free energies of reactions (20) and (21) are the highest, and the standard free energies of reactions (14) and (15) are in

Fig. 2 displays the standard free energy of equations (7) through (21). The thermodynamic data calculated using the FactSage software (Eqs. (7), (10), (13), (16) and (19)) indicates that Na_2SO_4 is difficult to react with SiO_2 and Al_2O_3 in the absence of CO and H_2 . When CO or H_2 is present, sodium modify reactions (Eqs. (8), (9), (11), (12), (14), (15), (17), (18), (20) and (21)) have much lower free energies by

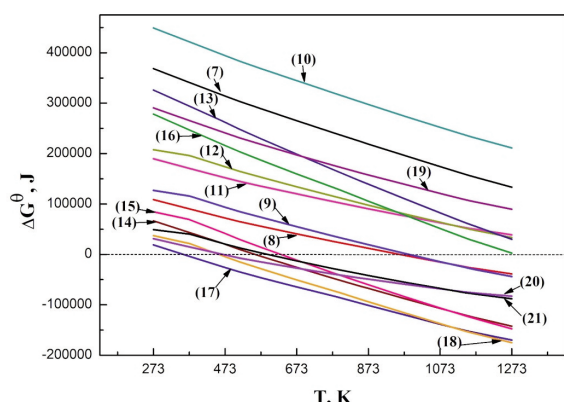


Figure 2. ΔG^0 -T results of equations (7) through (21)

Table 1. Chemical composition of pyrite cinder (wt %)

TFe	FeO	SiO ₂	Al ₂ O ₃	CaO	MgO	K ₂ O	Na ₂ O	P	S	LOI
62.95	11.57	5.62	2.08	0.45	0.31	0.23	0.028	0.035	0.39	1.02

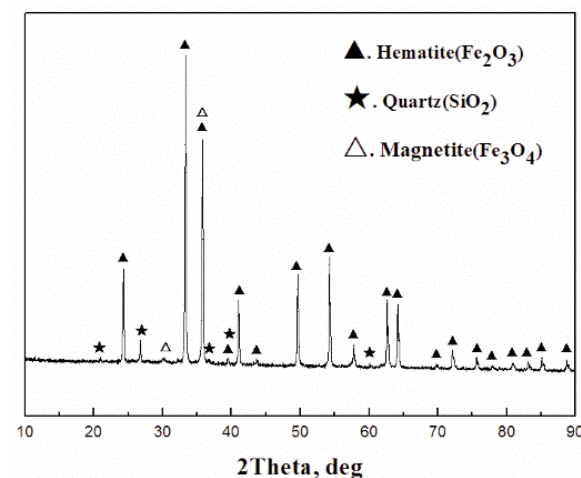


Figure 3. X-ray diffraction analysis of pyrite cinder

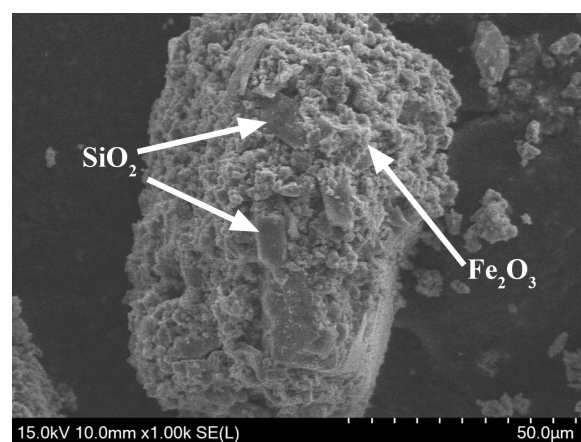
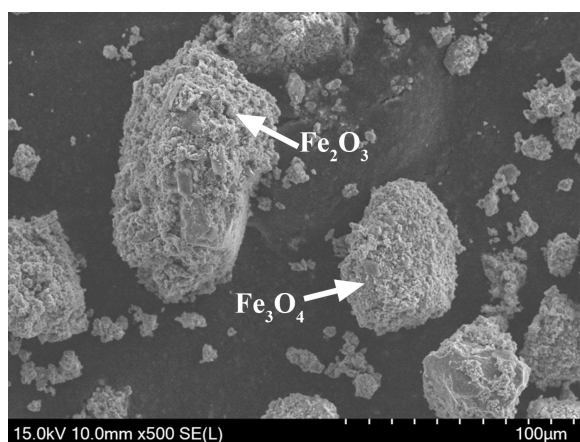


Figure 4. Microstructure (SEM) of pyrite cinder



the middle. Therefore, the gangue can be modified by Na_2SO_4 in pyrite cinder, and the most likely products are NaAlSiO_4 and $\text{NaAlSi}_3\text{O}_8$ after carburization.

3. Materials and methods

3.1 Raw Material

Pyrite cinder and an analytical reagent of Na_2SO_4 powder were used. The gases used were CO 99.95% purity, CO_2 99.99% purity, H_2 99.99% purity, and N_2 99.99% purity. The pyrite cinder's chemical composition is shown in Table 1. For the pyrite cinder fineness, the ratios were 72.58% ($< 0.075\text{mm}$) and 56.06% ($< 0.045\text{mm}$). The XRD result in Figure 3 displays that the main minerals in pyrite cinders are hematite, magnetite and quartz. It is illustrated in Figure 4 that the pyrite cinder particles own porous structure which benefits the gas diffusion during the carburization process.

3.2. Experimental methods

The flowsheet diagram of the process is listed in Fig. 5.

The methods of the pelletizing and preheating procedures were the same as in the literature [13]. In this study, the diameter of green ball was 8 to 10 mm.

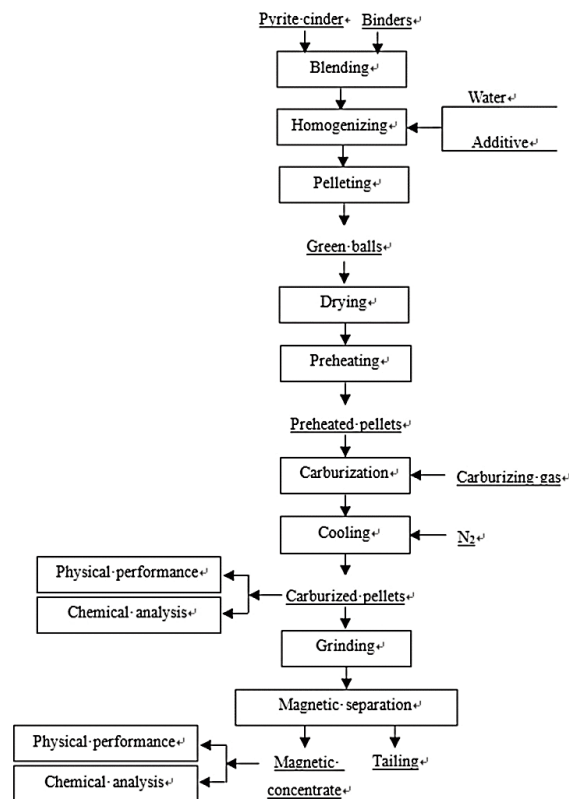


Figure 5. The flowsheet diagram of the process

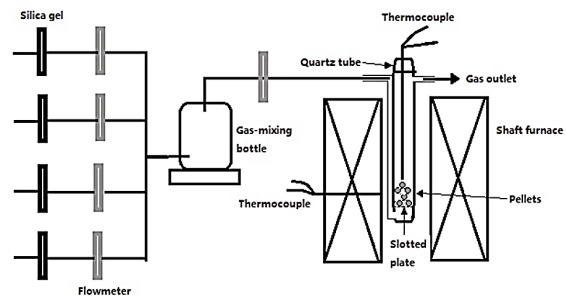


Figure 6. The schematic of the carburizing apparatus

The preheating temperature was $1000\text{ }^\circ\text{C}$, and the preheating time was 15 minutes. In addition, the size of furnace's alundum tube was $\Phi 80 \times 1200\text{ mm}$.

The carburization test was performed in a shaft furnace. Fig. 6 displays the schematic diagram of the carburizing apparatus. About 40g preheated pellets were put in a quartz tube ($\Phi 40 \times 600\text{ mm}$), and that quartz tube was inserted into the shaft furnace. Purified N_2 gas was introduced in the quartz tube at 1L/min for 10min. After that, purified CO (900ml/min), CO_2 (300ml/min), and H_2 (300ml/min) gases were mixed and introduced in the quartz tube for prescribed time. The carburized pellets were cooled to room temperature by N_2 gas at 1L/min when the carburization finished.

The descriptions of the grinding and magnetic separation processes can be found in the literature [1]. The carburized pellets were crushed to size less than 1mm, and then 20g sample was ground in a conical mill ($\Phi 160 \times 60$) with 50% pulp density. After that, the pulp was magnetically separated in a magnetic tube with a magnetic field intensity of 130 mT.

Chemical analysis standard of iron was carried out using ISO 2597-1-2006. The carbon content was detected using carbon-sulfur infrared analyzer. The sample used to detect free carbon reacted with nitric acid and hydrofluoric acid, which were used to remove the combined carbon. Then, the solution was suction filtration using acid-washed asbestos in a gooch crucible, and filter cake was washed by sodium hydroxide solution and hydrochloric acid. Dried filter cake mixed with acid-washed asbestos was used to detect the free carbon, using carbon-sulfur infrared analyzer. Other analysis devices included optical microscopy, XRD, SEM-backscattered electron (BSE) imaging, and energy-dispersive spectrometry (EDS).

4. Results and discussion

4.1. Influences of carburizing temperature

The influence of carburizing temperature can be found in Fig. 7. The content of iron significantly increases with the increasing carburizing temperature,



while the total carbon content, combined carbon content, and free carbon content of pellets drop remarkably. From Figs. 1 and 8, it is identified that the Fe_3O_4 is directly carburized to Fe_3C at 550 °C, which leads to the high content of Fe_3O_4 . Higher content of Fe_3O_4 results in the lower iron content. In addition, high content of Fe_3O_4 will be adverse to the recovery of iron from pyrite cinder in magnetic separation, because the saturation magnetization of Fe_3O_4 (92emu/g) is much lower than that of Fe_3C (150emu/g). When the temperature is in the range of 593 °C (866 K) to 678 °C (951 K) (Fig. 1), the Fe_3O_4 is reduced to FeO, and then the FeO is carburized to Fe_3C . However, due to the low conversion rate of FeO to Fe_3C [28], the FeO continues to be reduced to Fe, and then the Fe is carburized to Fe_3C (Fig. 8). Therefore, the final carburizing products are Fe_3C and metallic iron with a small amount at the temperature over 593 °C. The saturation magnetization of the metallic iron (210emu/g) is higher than that of Fe_3C , which favors the recovery of iron from pyrite cinder in magnetic separation. When the temperature is in the range of 678 °C (951 K) to 731 °C (1004 K) (Fig. 1), the FeO is reduced to Fe, and then the Fe is carburized to Fe_3C (Fig. 8). When the temperature is over 731 °C (1004 K), the product of the reduction and carburization in this study is metallic iron (Fig. 1), so the carbon content is very low at 750 °C (Fig. 7), and the carburized product is almost metallic iron (Fig. 8). In addition, according to the reports [33, 34], it is the chemical reaction that controls the reduction of iron ore pellet at the temperature range of 550 °C to 750 °C. Therefore, reduction rates of reactions (1) – (3) are improved by the high temperature. From Fig. 8, it can be seen that metallic iron content dramatically rises with the increasing temperature, so the iron content of the pellets significantly increases. From Fig. 1, it is

demonstrated that lower temperature favors producing more iron carbide, which is consistent with the result of this experiment (Fig. 7). However, more free carbon

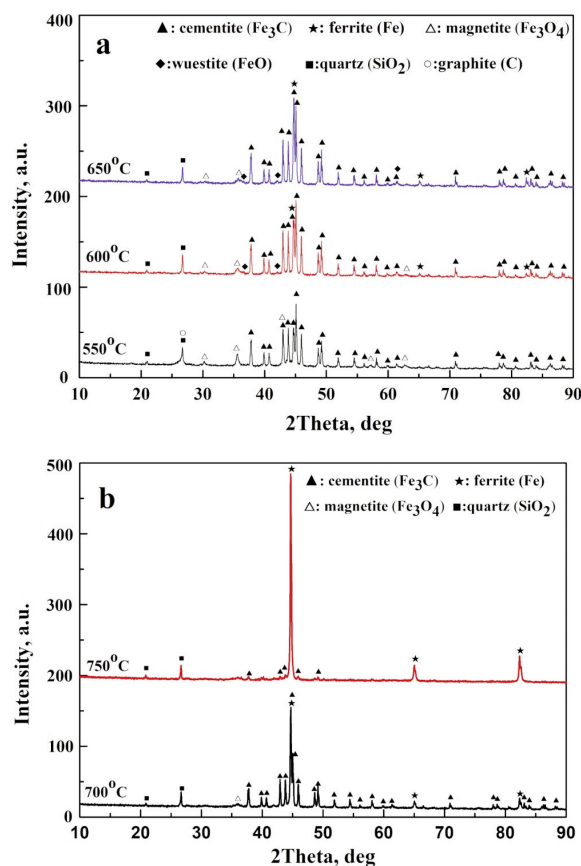


Figure 8. X-ray diffraction pattern of the carburizing pellets at different temperatures for 150min. The phases are identified as follows: Fe_3C is cementite, Fe is ferrite, Fe_3O_4 is magnetite, SiO_2 is quartz, and C is graphite

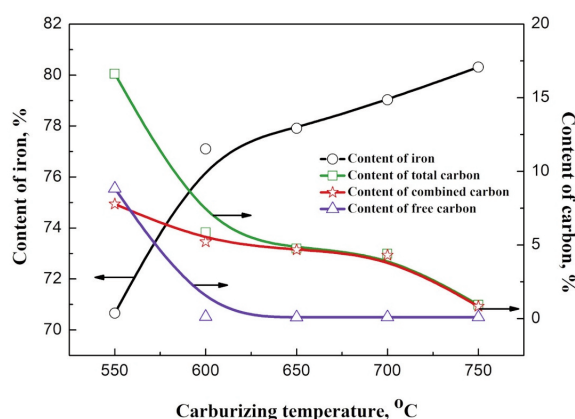


Figure 7. Effects of the carburizing temperature on the iron content, total carbon content, combined carbon content and free carbon content of the carburizing pellets (carburization for 150min)

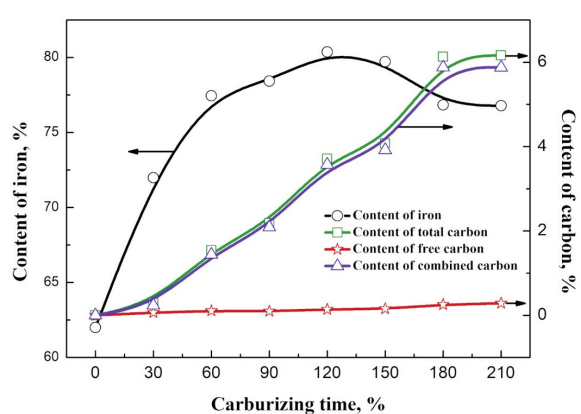


Figure 9. Effects of the carburizing time on the iron content, total carbon content, combined carbon content and free carbon content of the carburizing pellets (carburization at 650 °C)

is produced at lower temperature, especially at 550 °C (Fig. 7). Therefore, the appropriate carburizing temperature range is between 600 °C and 650 °C.

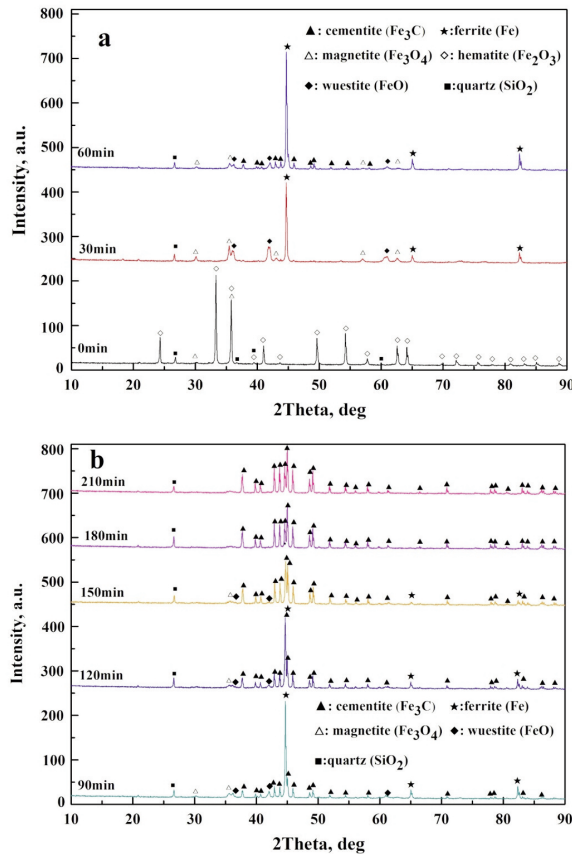


Figure 10. X-ray diffraction pattern of the carburizing pellets at 650 °C for different time. The phases are identified as follows: Fe_3C is cementite, Fe is ferrite, Fe_2O_3 is hematite, Fe_3O_4 is magnetite, and SiO_2 is quartz

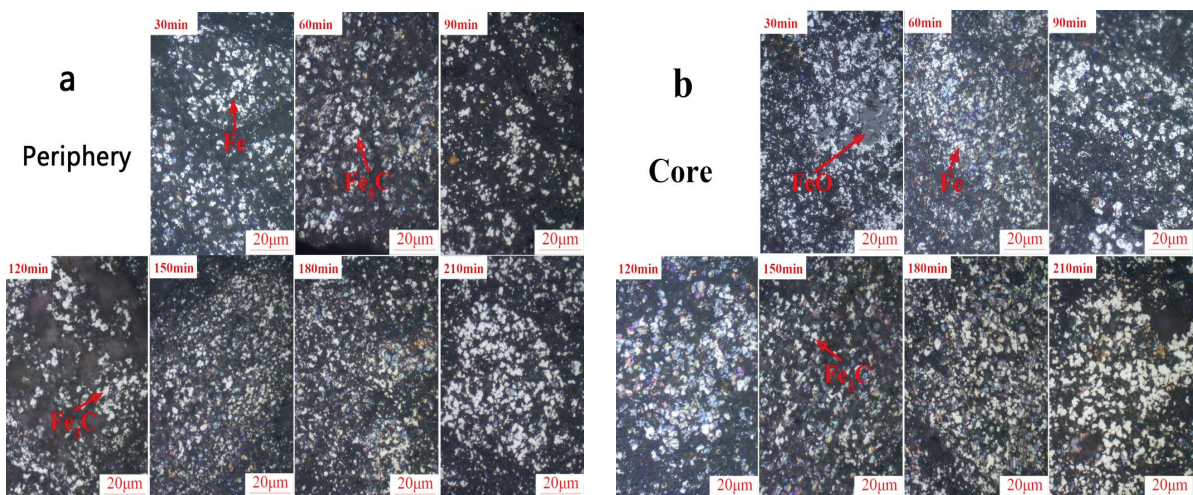


Figure 11. Microstructures of the (a) periphery and (b) core of pellets carburized at 650 °C for different time (wustite – gray, metallic iron – bright white, iron carbide – white, pore – black)

4.2. Influences of carburizing time

The influence of carburizing time is identified in Fig. 9. The content of iron significantly increases with the increasing carburizing time, while the iron content drops when the carburizing time is over 120 min. Reduction of iron oxide is the main reaction at the initial carburization stage (0-60min), because reduction rate of pellets is much faster than carburization rate of pellets [35]. Thus, metallic iron is the main phase in pellets (Fig. 10), especially in the core of pellets (Fig. 11), and the iron content dramatically increases at the initial stage. At the middle stage of carburization (between 60 min and 150 min), the carburization enhances and the reduction weakens, which leads to the slow rise of iron content. In addition, most of the metallic iron is carburized to iron carbide, so metallic iron content remarkably decreases, and iron carbide significantly increases (Fig. 10). Reduction and carburization are gradually accomplished (Fig. 10) at the late carburization stage (between 150 min and 210 min).

When the carburizing time exceeds 150 min, metallic iron almost disappears, and iron carbide increases slowly (Fig. 10), which leads to the decrease of iron content. Furthermore, the size of iron carbide particles significantly grows up (Fig. 11). The large particles of the iron carbide will promote the separation of iron carbide from gangue. The free carbon content slightly increases with the increasing carburizing time. When the carburizing time increases from 0 min to 210 min, the free carbon content only increases from 0% to 0.29%, while the combined carbon increases from 0% to 5.88%.

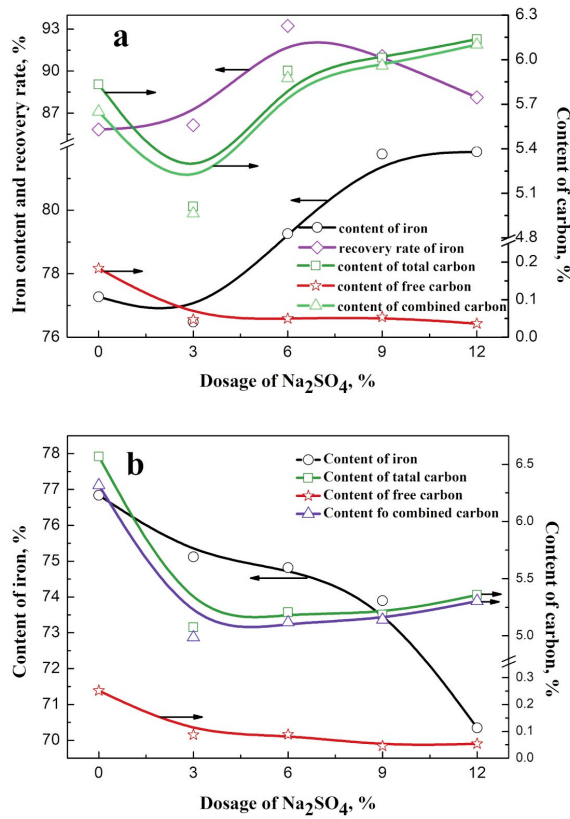


Figure 12. Effects of the Na_2SO_4 dosage on (a) the iron content, iron recovery rate, total carbon content, free carbon content and combined carbon content of the magnetic concentrate, and (b) the iron content, total carbon content, free carbon content and combined carbon content of the carburized pellets (carburization at 650°C for 180min, grinding fineness is 92.25% less than 0.025mm)

4.3. Influence of Na_2SO_4 dosage

The influence of Na_2SO_4 dosage is displayed in Fig. 12. The iron content of magnetic concentrate indicates an uptrend with the increasing Na_2SO_4 dosage. It is because the carbide particles are larger

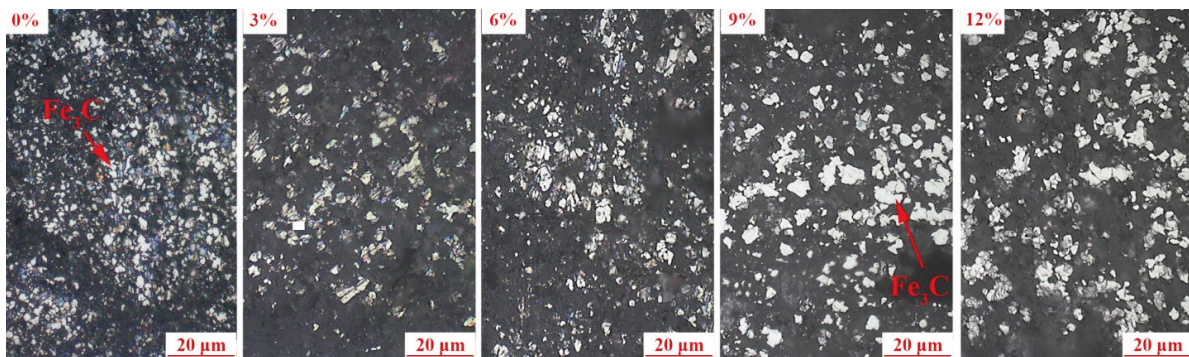


Figure 13. Microstructures of the pellets carburized at 650°C for 180min with different Na_2SO_4 dosage (iron carbide - white, pore-black)

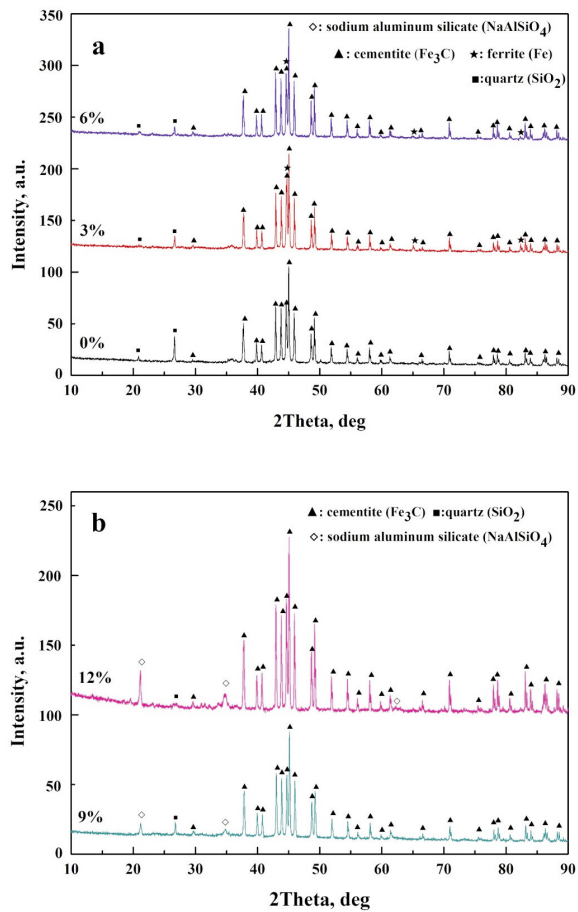


Figure 14. X-ray diffraction pattern of the carburizing pellets at 650°C for 180min. The phases are identified as follows: Fe_3C is cementite, Fe is ferrite, NaAlSiO_4 is sodium aluminum silicate, and SiO_2 is quartz

with more Na_2SO_4 additive (Fig. 13). During the preheating (1000°C), liquid Na_2SO_4 improves the diffusion coefficient of the iron ion, which promotes solid phase diffusion and formation of new crystalline bridge among iron oxide inside pellets [36]. New crystalline bridge continues to develop

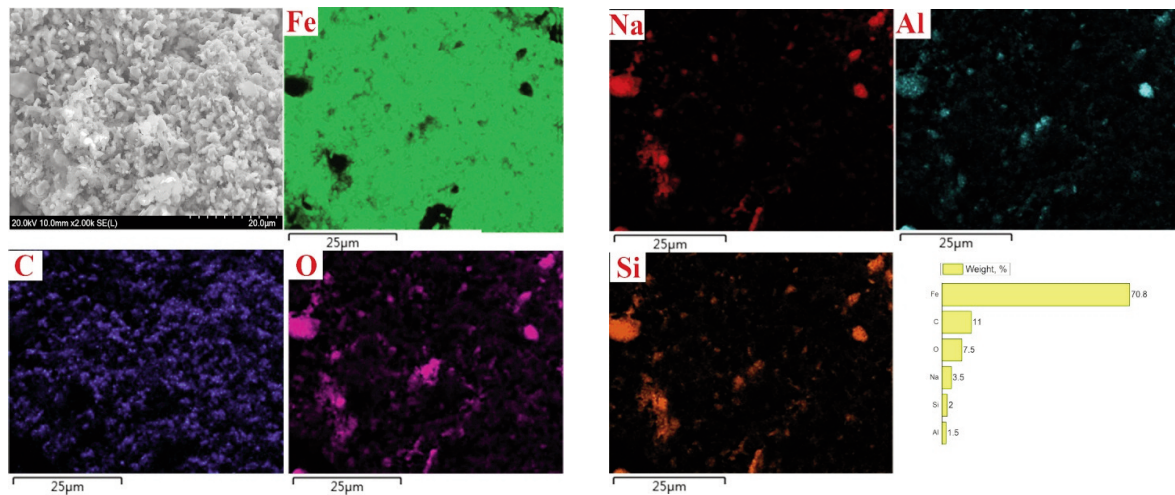


Figure 15. SEM image and elemental surface scanning of the carburized pellets at 650 °C for 180min with 9% Na_2SO_4

and grow during the carburization process, which produces large iron carbide particles. On the other hand, Na_2SO_4 reacts with Al_2O_3 and SiO_2 (Figs. 2 and 14) during the carburization process, which brings Al_2O_3 and SiO_2 together (Fig. 15) and makes them transform to new sodium salts. The new sodium salts change the embedment relationship of iron minerals and gangue to promote the separation of iron carbide from gangue. The iron recovery rate increases with an increase in Na_2SO_4 dosage, while the iron recovery rate drops when the Na_2SO_4 dosage is over 6%. When the Na_2SO_4 is added in pellets, Na_2SO_4 liquid blocks up the hole inside the pellets in preheating, which hinders the CO diffusion during the carburization, so the combined carbide reduces and the metallic iron appears (Figs. 12b and 14). However, separation of metallic iron

from gangue is easier than separation of iron carbide from gangue, and iron carbide particles grow up with adding Na_2SO_4 (Fig. 13). Both are the reasons of the increment of iron recovery rate. When the Na_2SO_4 dosage is over 6%, more iron oxides covered by gangue expose to the CO and H_2 gas due to the reactions of liquid Na_2SO_4 with gangue, which results in the increase of combined carbon content (Fig. 12b). In addition, more Na_2SO_4 leads to more SO_2 gas, due to the reactions (7) through (21). Sulfur depresses the precipitation of free carbon during the carburization [35], which causes the dramatic decrease of the free carbon content (Fig. 12). However, high dosage of Na_2SO_4 leads to the great rise of gangue content and the significant drop of iron content, which hinders the separation of iron carbide and gangue, so the dissociation degree

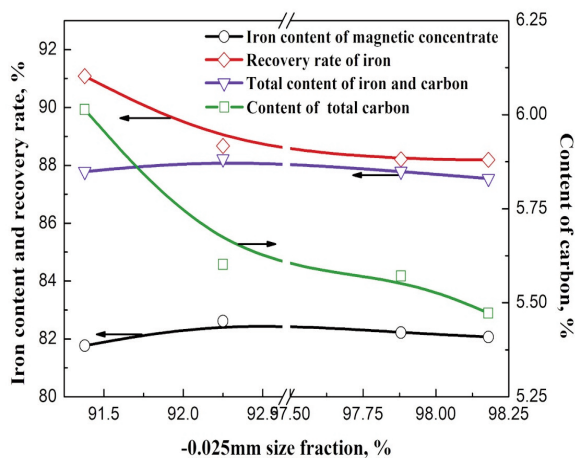


Figure 16. Effects of the grinding fineness on the iron content, iron recovery rate, total iron and carbon content, and carbon content of the magnetic concentrate at 650 °C for 180 min with 9% Na_2SO_4

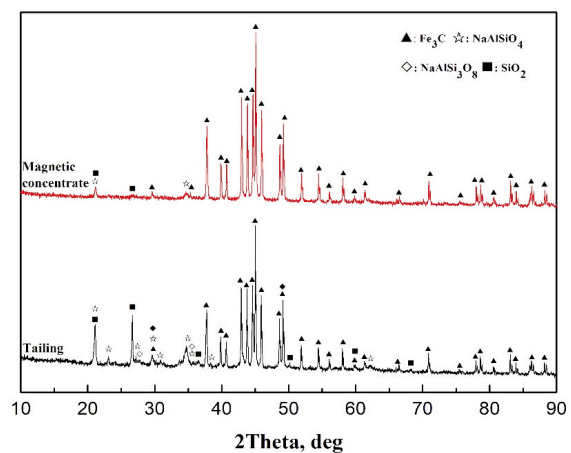


Figure 17. XRD patterns of the magnetic concentrate and tailing. The phases are identified as follows: Fe_3C is cementite, NaAlSiO_4 is sodium aluminum silicate and nepheline, $\text{NaAlSi}_3\text{O}_8$ is albite, and SiO_2 is quartz

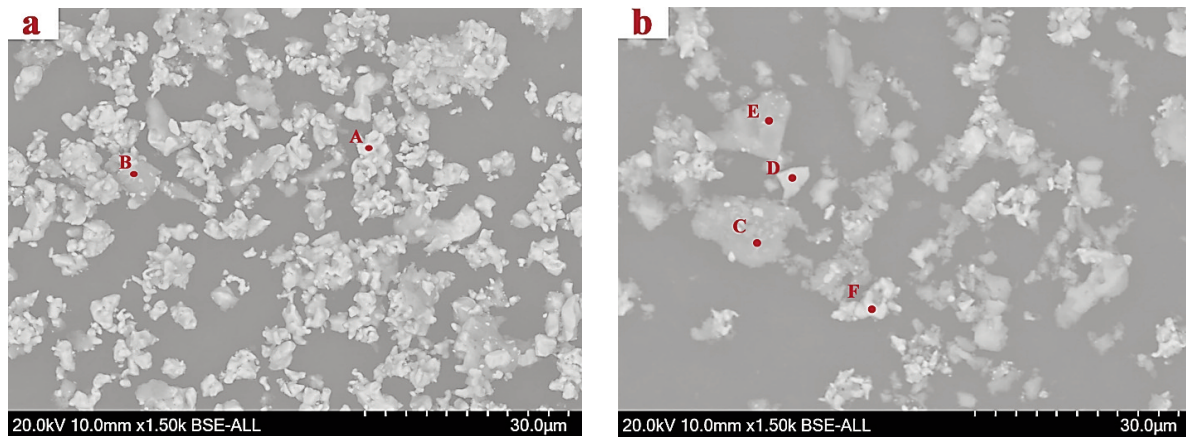


Figure 18. Products images under SEM (a: magnetic concentrate; b: tailing)

Table 2. Analysis results (EDS) of the products (wt %)

Composition	Fe	C	O	Si	Al	Na	Ca	Mg	Mn	Zn	K	Ti	S
Area A	76.7	22.6	/	0.3	0.4	/	/	/	/	/	/	/	/
Area B	9.6	/	42.6	17.7	13.8	12.4	0.2	0.7	0.5	0.7	1.4	/	0.4
Area C	13.7	/	41.8	16.6	0.7	20	3.4	0.5	2.8	/	/	/	0.5
Area D	70.5	/	25.4	1.1	0.8	1.9	0.1	/	/	/	/	/	0.2
Area E	11.2	/	43.3	17.2	7.5	14.3	1.3	0.9	1.7	1.5	0.3	0.1	0.7
Area F	64.5	25	7.2	0.7	0.6	1.6	0.1	/	/	/	/	/	0.3

of iron carbide and gangue reduces. Therefore, the iron recovery rate decreases when the dosage of Na_2SO_4 is over 6%.

4.4. Influences of grinding fineness

Fig. 16 shows the effects of grinding fineness on magnetic concentrate. It can be seen that iron carbide grain is very fine because recrystallization of iron minerals difficultly proceeds at the carburizing temperature [36], which leads to exceeding fine magnetic concentrate particles after ball-milling treatment comparing to the ordinary iron ore [1]. The iron content of magnetic concentrate slightly increases with the increasing grinding fineness, while the iron content decreases when the size fraction is higher than 92.25%. With the increasing grinding fineness, liberation degree of iron carbide and gangue goes up, which improves the iron content of magnetic concentrate. However, the increasing grinding fineness also results in the size drop of iron carbide particle. Fine particles cause the aggregation easily, which leads to the decrease of the iron recovery rate in magnetic separation [37]. When the size fraction continues to increase, both the iron content and iron recovery rate show downtrends, due to the enhanced particles

aggregation. When the size fraction is 92.25%, the total content of iron and carbon reaches to 88.22%.

4.5. Product analysis

The magnetic concentrate and tailing were prepared by carburizing at 650 °C for 180 min with 9% Na_2SO_4 .

From Fig. 17, it can be seen that iron carbide is the main phase in the magnetic concentrate, and also there are a small number of quartzs and sodium aluminum silicates, which identifies high quality magnetic concentrate. The gangues are dominated by quartz, albite, sodium aluminum silicate, and nepheline in the tailing, which demonstrates a good result of sodium modify.

Fig. 18 displays the images of the products. It can be concluded that the iron carbide particle is very fine in the magnetic concentrate, due to the poor toughness and fine grain. Most of the iron carbide (the white area) and gangue (the gray area) liberate well. A small number of fine iron carbides are covered by sodium salt (area B). It is the reason that the iron carbide further dissociates from gangue hardly. The XRD (Fig. 17) and EDS (Table 2) results demonstrate that the main compounds in areas C and E are albite, sodium aluminum silicate, and nepheline, and the

main compound in area D is iron oxide. From the Fig. 18(b), owing to particle aggregation during the magnetic separation process, a small number of fine iron carbide particles (area F) are mixed with gangue in the tailing.

5. Conclusions

1. The carburization-magnetic separation technique was verified effectively to prepare the high-grade iron carbide from pyrite cinder. By applying the carburization, iron carbide pellet was produced, and then iron carbide was upgraded by separation of iron carbide from gangue with wet ball-milling and magnetic separation.

2. The Na_2SO_4 is an effective additive, which significantly promotes the separation of iron carbide from gangue. During the preheating and carburization, Na_2SO_4 reacts with gangue minerals (Al_2O_3 and SiO_2) to form the new sodium salts, which increases the liberation degree of iron carbide and gangue. In addition, Na_2SO_4 improves the size growth of iron carbide particles, which makes the liberation of iron carbide easier.

3. The effects of the carburizing temperature, carburizing time, Na_2SO_4 dosage, and grinding fineness on carburized pellet and magnetic concentrate were investigated. The optimized process conditions were obtained as follows: carburization at 650 °C for 180 min, Na_2SO_4 dosage of 9% and the grinding fineness of 92.25% powder passing 0.025mm. Under these conditions, for the magnetic concentrate, the total iron and carbon content reached 88.22%, and the rate of iron recovery reached 88.67%.

Acknowledgement

This work was supported by the National Natural Science Foundation of China (NO. 51504155).

References

- [1] D. Chen, H. Guo, J. Xu, Y. Lv, Z. Xu, H. Huo, *Metall. Mater. Trans. B*, 48 (2017) 933-942.
- [2] T. Vamerali, M. Bandiera, L. Coletto, F. Zanetti, N.M. Dickinson, G. Mosca, *Environ. Pollut.*, 157 (2009) 887-894.
- [3] C. Yang, Y. Chen, P.A. Peng, C. Li, X. Chang, Y. Wu, *J. Hazard. Mater.*, 167 (2009) 835-845.
- [4] E.P. Li, Y.Q. Qiu, R.J. Xiang, Y.X. Cheng, *Min. Metall. Eng.*, 34 (2014) 79-82.
- [5] M. Giunti, D. Baroni, E. Bacci, *Bull. Environ. Contam. Toxicol.*, 72 (2004) 352-357.
- [6] D.V. Kerkez, M.R. Becelic-Tomin, M.B. Dalmacija, D.D. Tomasevic, S.D. Roncevic, G.V. Pucar, B.D. Dalmacija, *Hem. Ind.*, 69 (2015) 231-239.
- [7] S. Panda, A. Akcil, S. Mishra, C. Erust, *J. Hazard. Mater.*, 325 (2017) 59-70.
- [8] Y. Zheng, Z. Liu, *Powder Technol.*, 207 (2011) 335-342.
- [9] J. Tian, L.H. Xu, W. Deng, H. Jiang, Z.Y. Gao, Y.H. Hu, *Chem. Eng. Sci.*, 164 (2017) 99-107.
- [10] I.V. Kovkov, V.Z. Abdrakhimov, *Glass Ceram.*, 68 (2011) 128-130.
- [11] D. Wu, Y. Liu, H. He, Y. Zhang, *Chemosphere*, 155 (2016) 127-134.
- [12] S. Zhang, S. Rajendran, S. Henderson, D. Zeng, R. Xiao, S. Bhattacharya, *Energ. Fuel.*, 29 (2015) 2645-2655.
- [13] D. Chen, D.Q. Zhu, Y. Chen, *ISIJ Int.*, 54 (2014) 2162-2168.
- [14] D.Q. Zhu, T.J. Chun, J. Pan, Z.Q. Guo, *Ironmak. Steelmak.*, 40 (2013) 430-435.
- [15] X.H. Fan, Q. Deng, M. Gan, H.B. Wang, *J. Iron Steel Res. Int.*, 22 (2015) 371-376.
- [16] J. Gao, W. Wang, A.J. Rondinone, F. He, L. Liang, *J. Hazard. Mater.*, 300 (2015) 443-450.
- [17] H. Wang, G. Li, J. Ma, D. Zhao, *RSC Adv.*, 7 (2017) 3921-3927.
- [18] D.Y. Wang, C.J. Liu, M.F. Jiang, *New Steelmaking Raw Material-Characterization and Preparation Techniques of Iron Carbide*, Science Press, Beijing, 2012, p. 68-88 (In Chinese).
- [19] D. Chaira, B. Mishra, S. Sangal, *J. Alloys Compd.*, 474 (2009) 396-400.
- [20] P. Zhang, L. Bi, D. Zhang, X. Wang, W. Wang, X. Lei, H. Yang, *Mater. Res. Bull.*, 76 (2016) 327-331.
- [21] B. David, O. Schneeweiss, E. Santava, Morjan, *Acta Phys. Pol. A*, 118 (2010) 766-767.
- [22] R. Miyatani, Y. Yamada, Y. Kobayashi, *J. Radioanal. Nucl. Chem.*, 303 (2015) 1503-1506.
- [23] J.A. Nelson, M.J. Wagner, *Chem. Mater.*, 14 (2002) 4460-4463.
- [24] Y. Man, Z. Chen, Y. Zhang, P. Guo, *Mater. Design*, 97 (2016) 417-423.
- [25] H. Yumoto, Y. Nagamine, J. Nagahama, M. Shimotomai, *Vacuum*, 65 (2002) 527-531.
- [26] S. Cetinkaya, S. Eroglu, *Int. J. Miner. Process.*, 152 (2016) 46-52.
- [27] M. Kazemi, D. Sichen, *Metall. Mater. Trans. B*, 47 (2016) 3519-3526.
- [28] A.N. Conejo, G.P. Martins, *ISIJ Int.*, 37 (1997) 967-976.
- [29] D.Y. Kim, Y.U. Heo, Y. Sasaki, *ISIJ Int.*, 53 (2013) 950-957.
- [30] J. Yu, Y. Han, Y. Li, P. Gao, *J. Min. Metall. Sect. B-Metall.*, 54 (1) B (2018) 21-27.
- [31] J. Xiang, Q. Huang, X. Lv, C. Bai, *J. Hazard. Mater.*, 336 (2017) 1-7.
- [32] Y. Lei, Y. Li, W. Chen, R. D. Wang, *ISIJ Int.*, 57(2017)



- 791-794.
- [33] Y.B. Gao, H.G. Kim, H.Y. Sohn, Trans. Inst. Min. Metall. C, 121 (2012) 109-116.
- [34] G.Z. Qiu, T. Jiang, J.C. Xu, N.Z. Cai, Direct Reduction of Cold-Bonded Pellets, Central South University Press, Changsha, 2001, p. 193 (In Chinese).
- [35] Y. Iguchi, K. Hori-I, T. Shibata, S. Hayashi, ISIJ Int., 44 (2004) 984-991.
- [36] T. Jiang, Principle and Technology of Agglomeration of Iron Ores, Central South University Press, Changsha, 2016, p. 215 (In Chinese).
- [37] L. Luo, A.V. Nguyen, Sep. Purif. Technol., 172 (2017) 85-99.

PRIPREMA I DOBIJANJE KARBIDA GVOŽĐA OD ŠLJAKE PIRITA KORIŠĆENJEM KARBURIZACIJE I TEHNOLOGIJE MAGNETNE SEPARACIJE

D. Chen^{a*}, H. Gou^a, Y. Lv^b, P. Li^a, B. Yan^a, J. Xu^a

^a Fakultet za gvožđe i čelik, Univerzitet Sudžu, Džangsu, Kina

^b Odsek za mašinstvo i elektrotehniku, Institut za industrijsku tehnologiju Sudžu, Džangsu, Kina

Apstrakt

Nova tehnika karburizacije posle koje sledi magnetna separacija predstavljena je za pripremu visokokvalitenog karbida gvožđa od šljake pirita da bi se unapredila upotreba šljake pirita sa visokom dodatom vrednošću. Istraživani su efekti temperature karburizacije, vreme karburizacije i doziranje Na_2SO_4 na karburizovani pelet, kao i efekti doziranja Na_2SO_4 i finoća mlevenja magnetnog koncentrata. Predloženi su sledeći optimizirani parametri procesa: karburizacija na 650°C u trajanju od 180 minuta u $\text{CO-CO}_2\text{-H}_2$ mešavini gasova, doziranje Na_2SO_4 od 9%, intenzitet magnetnog polja 130 mT, i finoća mlevenja gde je 92.25% praha 0.025mm. Sadržaj gvožđa, ukupan sadržaj karbida, ukupan sadržaj gvožđa i karbida magnetnog koncentrata bili su 82.62%, 5.60%, i 88.22%. Stopa dobijanja gvožđa dostigla je 88.67%. Ponašanje i mehanizmi karburizacije, separacije, i Na_2SO_4 potvrđeni su uz pomoć optičke mikroskopije, XRD, i SEM.

Ključne reči: Šljaka pirita; Karbid gvožđa; Karburizacija; Magnetna separacija

